Impact of saturation on the polariton renormalization in III-nitride based planar microcavities

Georg Rossbach,* Jacques Levrat, Eric Feltin,† Jean-François Carlin, Raphaël Butté, and Nicolas Grandjean
Institute of Condensed Matter Physics, École Polytechnique Fédérale de Lausanne (EPFL), CH-1015 Lausanne, Switzerland
(Received 21 June 2013; revised manuscript received 12 September 2013; published 21 October 2013)

It has been widely observed that an increasing carrier density in a strongly coupled semiconductor microcavity (MC) alters the dispersion of cavity polaritons, below and above the condensation threshold. The interacting nature of cavity polaritons stems from their excitonic fraction being intrinsically subject to Coulomb interactions and the Pauli-blocking principle at high carrier densities. By means of injection-dependent photoluminescence studies performed nonresonantly on a GaN-based MC at various temperatures, it is shown that already below the condensation threshold saturation effects generally dominate over any energy variation in the excitonic resonance. This observation is in sharp contrast to the usually assumed picture in strongly coupled semiconductor MCs, where the impact of saturation is widely neglected. These experimental findings are confirmed by tracking the exciton emission properties of the bare MC active medium and those of a high-quality single GaN quantum well up to the Mott density. The systematic investigation of renormalization up to the polariton condensation threshold as a function of lattice temperature and exciton-cavity photon detuning is strongly hampered by photonic disorder. However, when overcoming the latter by averaging over a larger spot size, a behavior in agreement with a saturation-dominated polariton renormalization is revealed. Finally, a comparison with other inorganic material systems suggests that for correctly reproducing polariton renormalization, exciton saturation effects should be taken into account systematically.

DOI: 10.1103/PhysRevB.88.165312 PACS number(s): 71.36.+c, 78.67.Pt, 78.67.De, 42.55.Sa

I. INTRODUCTION

One of the most striking features of exciton polaritons, which originate from the strong coupling between a confined photonic mode and an excitonic resonance, is their ability to interact via their matter component. This allows an efficient thermalization and eventually the formation of a condensate in the center of the Brillouin zone,[1–4] when overcoming relaxation bottleneck issues.[5] However, it is worth mentioning that the polariton properties and interactions are not invariant, but can be significantly altered when the carrier density is increased owing to the renormalization of the exciton transition. In particular, the exciton energy E_X, its corresponding homogeneous linewidth γ_X, and oscillator strength $f_{osc,X}$ are affected by the combined effects of Coulomb interaction, via direct and exchange terms, and phase-space filling.[6] Within the standard picture, particularly applied to GaAs- and CdTe-based microcavities (MCs), it is usually assumed that the polariton renormalization is exclusively governed by Coulomb interaction and the impact of the saturation terms is often neglected.[3,7,8] However, for the case of wide band-gap semiconductors such as ZnSe, GaN, or ZnO, the excitonic properties are remarkably different. In particular, we can point out their increased exciton oscillator strength and binding energy, and their reduced Bohr radius and static dielectric constant.[9–11] Hence, one can naturally expect exciton and polariton renormalization to be also strongly modified compared with more conventional systems. Another aspect, which has to be taken into account, comes from the fact that the reduced exciton size implies a generally increased sensitivity to alloy disorder and crystal imperfections resulting in a considerably increased inhomogeneous linewidth.

Eventually, a better understanding of the origin of polariton renormalization, below and above the condensation threshold, is of major importance for gaining a deeper insight into the polariton condensate formation and the occurrent interaction mechanisms. Problems arise, for instance, when the ground-state population, a key parameter in the description of polariton condensates, is deduced on the basis of the emission energy shift at normal incidence δE_0.[8,12] This description is exclusively valid in the limit where δE_0 can be attributed to the density-dependent chemical potential $\mu(n_0)$, where n_0 is the polariton ground-state population. In the case where polariton renormalization originates from various sources, such an approach would inevitably lead to an overestimate of the condensate population. Additional effects have to be taken into account in particular when the blue-shift is caused by a large polariton reservoir population.[13,14] This could be caused either by a blue-shift of the exciton resonance as assumed in Ref. 13, or by a decrease of $f_{osc,X}$ due to saturation effects. These latter mechanisms might also have to be accounted for when considering polariton fluids:[15] a changing polariton dispersion will lead to a density- and spatially dependent polariton mass.

In this paper, we address the problem of polariton renormalization by investigating the impact of exciton-cavity photon detuning δ, temperature, spot size, and carrier density on the polariton energy by performing angle-resolved nonresonant photoluminescence (PL) experiments on a planar MC containing 67 homogeneously distributed GaN/$Al_{0.2}Ga_{0.8}N$ quantum wells (QWs). The low-injection vacuum Rabi splitting Ω of the present MC is about 60 meV, and δ values ranging between -120 and 10 meV are accessible. Contrary to the reported behavior of other systems, no significant blue-shift of the exciton, compared to its binding energy and Ω, could be tracked, but a decrease in Ω is commonly observed when increasing the carrier density up to the condensation threshold.[16]

II. SAMPLES AND EXPERIMENTAL DETAILS

In this work, we analyze the carrier-injection-dependent optical response of a multiple-QW (MQW) III-nitride based planar MC operating in the strong light-matter coupling regime (SCR) and showing polariton condensation up to room temperature. Detailed information on the metal-organic vapor phase epitaxy (MOVPE) grown structure and related previous experimental studies can be found elsewhere.[16–21] In order to investigate the impact of an increasing carrier density on the bare excitonic properties, we will also consider a single GaN QW structure and the bare active medium of the MC. The latter was deposited in the same run as the MC on a second template. Relevant information can be found in Ref. 18. The single 2-nm-thick GaN QW is sandwiched between two $Al_{0.15}Ga_{0.85}N$ barriers (30 nm on top and 200 nm below) and was grown on free-standing *c*-plane GaN substrate by MOVPE.

The optical response was probed by means of nonresonant PL measurements using either a pulsed frequency-quadrupled Nd:YAG laser [$\lambda = 266$ nm, repetition rate 8.52 kHz, pulse width 500 ps] for power-dependent measurements, or the frequency-doubled line of an Ar^+ laser [$\lambda = 244$ nm, continuous wave (cw)] for the micro-PL mapping. The eigenmode dispersion of the MC has been monitored using a UV microscope objective (numerical aperture NA = 0.55) focusing the Nd:YAG laser beam down to a spot diameter not larger than 5 μm. By the use of two lenses with respective focal lengths of 30 and 20 cm, the back focal plane of the objective (Fourier plane) was directly imaged on the entrance slit of the spectrometer. With the latter, a spectral resolution better than 150 μeV was reached via the combination of a 55-cm focal length monochromator and a liquid-nitrogen cooled CCD. Measurements with a larger spot size ($\sim$50 μm) have been carried out by introducing a 10-cm focal-length lens in the excitation line instead of the UV microscope objective. An optional 50-μm pinhole positioned in the focal plane of the first collection lens allowed us to select only the emission originating from the region with homogeneous and highest carrier density. For the micro-PL measurements, the Gaussian-shaped cw laser beam was sent through a UV microscope including the previously described UV objective and using a closed-loop piezostage for spatially resolved scans. This setup allows reaching a diffraction-limited spot size of $\sim$500 nm.

In addition, envelope-function calculations following a plane-wave expansion method have been conducted in order to determine the exciton binding energy and the impact of carrier density for the investigated structures.[22] The iterative Schrödinger-Poisson solver was found to be stable for carrier densities up to 1×10^{13} cm^{-2}. Appropriate material parameters were adopted from Ref. 23, while for the binding energy of QW excitons the approach described in Ref. 24 was followed.

III. EXCITONS IN THE HIGH-DENSITY REGIME

An exciton is composed of two fermionic particles, namely, an electron and a hole. It has an integer spin, which suggests that a dilute excitonic system should share very similar properties with a Bose gas.[25] In this section, we address the impact of the carrier density on the stability of the excitonic transition and the limits of the bosonic picture. With respect to the experimental investigations presented later in this work, we restrict ourselves to two-dimensional (2D) systems, i.e., QW excitons.

A. Validity of the bosonic picture and Mott transition

The creation operator $\hat{d}^\dagger(\mathbf{k}_\parallel)$ of an exciton with in-plane wave vector $\mathbf{k}_\parallel$ can be expressed as a linear combination of the uncorrelated electron and hole creation operators. A calculation of the commutator $[\hat{d}(\mathbf{k}_\parallel),\hat{d}^\dagger(\mathbf{k}'_\parallel)]$ for the $1s$ exciton state is a challenging task, but its mean value for a 2D system with exciton carrier density n_X can be expressed as[26,27]

$$[\hat{d}(\mathbf{k}_\parallel),\hat{d}^\dagger(\mathbf{k}'_\parallel)] = \delta_{\mathbf{k}_\parallel,\mathbf{k}'_\parallel} - \mathcal{O}\left(n_X a_B^2\right). \tag{1}$$

It turns out that the bosonic commutation rule is never completely satisfied for excitons and thus also for exciton polaritons, but a good agreement is achieved in the low-density regime, i.e., for densities $n_X \ll 1/a_B^2$, where a_B is the 2D exciton Bohr radius. This criterion does not define a clear frontier for the validity of the bosonic picture since the value of the commutator in Eq. (1) continuously decreases with injected carrier density.[28] Thereby, the loss of the bosonic character stems from the increasing role played by the fermionic exchange terms and the progressive filling of the phase space. This process can be followed up to a given critical carrier density n_X^{crit}, where the interparticle distances are so much reduced that the fermionic nature of the exciton constituents starts dominating: the binding energy vanishes and excitons are no longer stable particles. At this stage, usually referred to as the *Mott transition*,[29] the system should be described by an uncorrelated electron-hole plasma. Schmitt-Rink *et al.* theoretically estimated n_X^{crit} to be[6]

$$\frac{1}{n_X^{\mathrm{crit}}} \approx \frac{\pi a_B^2}{0.117} \tag{2}$$

for cold exciton screening. This value can additionally be modified by free electron-hole pair screening, which might even become dominant for GaAs QWs at elevated temperatures.[30] Nevertheless, it has been shown, both experimentally[31] and theoretically,[6,32] that screening due to free carriers and excitons should be of comparable strength in QWs. With respect to the large exciton binding energy of the QWs under investigation here, $E_X^b \sim 48$ meV,[18] we assume the impact of free electron-hole pairs to be negligible up to room temperature and thus throughout the paper, i.e., $n = n_X$.[21] It is further worth mentioning that the estimate of Eq. (2) lies almost one order of magnitude below the value given by the Pauli exclusion area $(1/\pi a_B^2)$, which emphasizes the large uncertainty in deriving an absolute n_X^{crit} value. While the Mott transition was initially claimed to be an abrupt first-order one, a point which is still theoretically debated,[33–35] experiments seem to be in favor of the continuous case in both two- and three-dimensional systems in agreement with Eq. (1).[36–39]

B. Excitonic nonlinearities

The optical response of a homogeneously broadened QW exciton ground state in the local approximation can be

described by a dielectric susceptibility of the form

$$\chi(E) \propto \frac{f_{\mathrm{osc,X}}}{E - E_{\mathrm{X}} + i\gamma_{\mathrm{X}}}. \quad (3)$$

Excitonic nonlinearities occur when at least one of these quantities scales with carrier density. Thereby, multiple physical effects have to be considered and shall be discussed in the following.

As the system intrinsically consists of charged particles, namely, electrons and holes, it is predominantly driven by Coulomb interactions. Both direct and exchange terms have to be taken into account and induce different effects. In a QW subject to a built-in electric field, direct Coulomb interaction of a rising carrier population progressively increases the transition energy by screening the field. At the same time, the increased electron and hole wave-function overlap will reinforce the exciton binding energy $E_{\mathrm{X}}^{\mathrm{b}}$ and $f_{\mathrm{osc,X}}$.[40] This so-called quantum-confined Stark effect (QCSE) is common for polar III-nitride heterostructures, where polarization discontinuities at the interfaces create huge built-in electric fields and the transition energy of QWs might even drop below the one of the bulk material.[41] Note that the blue-shift of the emission induced by the progressive screening of the internal field starts to play a role only for carrier densities higher than 10^{11} cm^{-2},[42] in agreement with calculations performed within this study.

Coulomb interactions are also expected to directly affect $E_{\mathrm{X}}^{\mathrm{b}}$. In pump-probe absorption experiments performed on a GaAs QW-based structure, E_{X} was found to shift to higher energy with increasing carrier density.[43] This effect was attributed to the predominantly repulsive interactions between excitons at elevated densities. Several corresponding theoretical investigations have been conducted. The majority of them expect a linear scaling of the excitonic blue-shift with carrier density[6,12,44]

$$\delta E_{\mathrm{X}} = E_{\mathrm{X}}^{\mathrm{b}} \frac{n_{\mathrm{X}}}{n_{\mathrm{X}}^{\mathrm{sat,1}}}, \quad (4)$$

up to a certain critical saturation density $n_{\mathrm{X}}^{\mathrm{sat,1}}$ given by Coulomb exchange interaction.[6]

Aside from the excitonic blue-shift, one also has to account for band-gap renormalization (BGR) induced by many-body interactions. The BGR red-shift is supposed to scale with the cubic root of the carrier density in two and three-dimensional systems, i.e., $\delta E_{\mathrm{BGR}} = -\alpha n^{1/3}$. The prefactor α is a material-, temperature-, and dimensionality-dependent constant.[36,45,46] It is also worth mentioning that BGR is expected to affect excitons and uncorrelated electron-hole pairs differently.[47,48]

Finally, taking into account the decrease in $E_{\mathrm{X}}^{\mathrm{b}}$ and BGR, the prediction of the evolution of the exciton transition energy with rising n_{X} appears to be a rather intricate task due to partial compensation of both effects with different power laws, especially when the QCSE comes additionally into play. Indeed, in most of the conducted time-resolved and time-integrated studies, only marginal or even negligible excitonic blue-shifts were recorded up to high densities.[36,39,49] These observations are confirmed by theoretical considerations, which revealed a remarkable independence of the exciton energy on the carrier injection up to the Mott density due to the exciton charge neutrality and thus an almost perfect compensation of BGR and exciton-exciton interactions.[32,35,36] Taking into account the shrinkage of the continuum band gap E_{G} due to BGR, a simplified criterion for $n_{\mathrm{X}}^{\mathrm{crit}}$ can also be set by

$$E_{\mathrm{G}}\left(n = n_{\mathrm{X}}^{\mathrm{crit}}\right) = E_{\mathrm{X}}(n = 0), \quad (5)$$

which in turn implies $n_{\mathrm{X}}^{\mathrm{crit}} \approx n_{\mathrm{X}}^{\mathrm{sat,1}}$.

Apart from the change in the resonance energy, Coulomb exchange interaction is also expected to influence $f_{\mathrm{osc,X}}$. Here, phase-space filling (PSF) becomes additionally effective: already occupied excited states can not be filled twice owing to the Pauli-blocking principle and thus do not contribute to absorption. Although different scalings for the $f_{\mathrm{osc,X}}$ saturation with carrier density have been proposed,[6,30,50] in view of polariton condensation a constant value due to low carrier injection is commonly assumed.[7,8,13,44] Here, we adopt an empirical saturation relation, which has been reported in several experiments:[30,51]

$$f_{\mathrm{osc,X}}(n_{\mathrm{X}}) = \frac{f_{\mathrm{osc,X}}(0)}{1 + n_{\mathrm{X}}/n_{\mathrm{X}}^{\mathrm{sat,2}}}, \quad (6)$$

where $f_{\mathrm{osc,X}}(0)$ is the exciton oscillator strength at zero carrier density, which approximately amounts to 5.1×10^{13} cm^{-2} in narrow GaN/(Al,Ga)N QWs.[18] Note that the oscillator strength saturation density $n_{\mathrm{X}}^{\mathrm{sat,2}}$ is not directly connected to the Mott density, but only states the density where $f_{\mathrm{osc,X}}$ is decreased to half its initial value. It should thus be significantly smaller than $n_{\mathrm{X}}^{\mathrm{crit}}$. The absolute ratio between them remains beyond the scope of this section and shall be discussed in Sec. V.

PL measurements performed under nonresonant excitation indicated that exciton-exciton interactions are also responsible for the collisional-induced broadening (CB) of the excitonic line.[44,52] In particular, it was shown that the excitonic line shape can be fitted by convoluting a Gaussian of constant linewidth $\gamma_{\mathrm{X}}^{\mathrm{inh}}$ accounting for disorder and a density-dependent Lorentzian of linewidth γ_{X}. The associated prefactor depends on the interparticle scattering efficiency and the power law appears to be linear or sublinear depending on the excitation conditions.[53]

In addition, nonidealities such as localization and sample heating might have to be considered. In the first case, the progressive filling of localization centers would lead to an apparent blue-shift of the exciton line in PL measurements, while the absorption spectrum and thus the intrinsic optical properties are not readily modified, given that the density of localized states is much lower than the saturation density. Due to the state-of-the-art quality of the QW set investigated here ($\gamma_{\mathrm{X}}^{\mathrm{inh}} \sim 11$ meV), this effect is expected to take place at densities far below those where QCSE screening and $E_{\mathrm{X}}^{\mathrm{b}}$ reduction appear. An increase in the lattice temperature due to local sample heating by the pump causes a red-shift in the emission and a potentially increased homogeneous linewidth. However, due to the low-duty cycle ($\sim 4 \times 10^{-6}$) used in our experiments, the impact of heat is kept at a minimum and we can safely neglect this contribution in the line-shape analysis.

C. GaN/AlGaN quantum wells under high injection

Investigating the Mott transition by means of PL measurements is a challenging task in many aspects. First, it constitutes an approach not exclusively probing intrinsic material

properties, but which is affected by carrier relaxation, thermal occupancy, and defect states, a combination of effects which has to be carefully considered. Nonetheless, PL is applied here for the sake of comparison with the MC structure and owing to the ease of carrier injection, even though another difficulty arises from the obvious need for homogeneity of the latter. Due to the finite absorption coefficient, the distribution of injected carriers shows a strong vertical gradient in both bulk and MQW based structures, which results in the simultaneous detection of a PL signal originating from highly and weakly injected regions. Another issue emerges from the combination of time-integrated measurements and a pulsed excitation source. From Ref. 21, the decay time of the exciton in the MQW structure is known to be close to the duration of the excitation pulse (500 ps) at low temperatures. Note that this exciton lifetime is strongly injection dependent due to the density dependence of $f_{\mathrm{osc,X}}$, the saturation of nonradiative recombination centers, and the impact of carrier localization. However, the relative proximity of both time scales implies that the recorded PL signal also represents a mixture of a high-density signal, when carriers are continuously supplied by the pump, and of the integrated decay of the decreasing carrier population at the end of each pulse. Accordingly, there will be an excitonic signature in the spectra even when the Mott transition has already been crossed during the pulse and the visibility of any exciton energy shift will be reduced. Nevertheless, the recorded spectra are expected to be dominated by the emission of the highly injected QWs. Thus, in order to guarantee an optimum comparability between the behavior of single and multiple GaN QWs and the full MC structure, we have chosen identical excitation conditions as stated in Sec. II including spatial filtering with a 50-μm pinhole.

Figure 1(a) displays a PL power series performed under nonresonant excitation conditions at 4 K on the GaN MQW structure representing the active medium of the MC. The

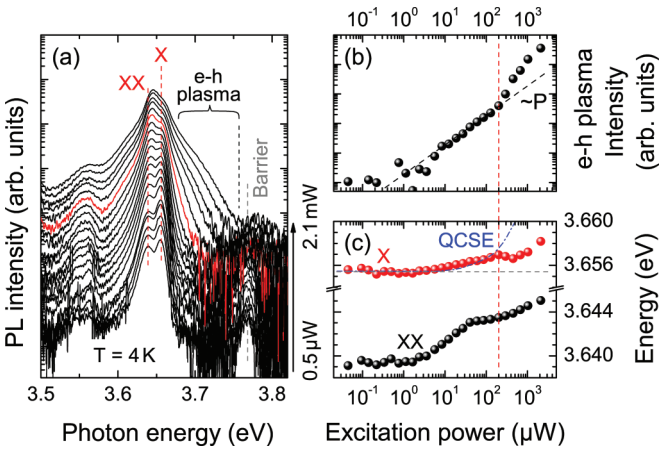

FIG. 1. (Color online) (a) PL power series recorded at 4 K on the GaN/$Al_{0.2}Ga_{0.8}N$ MQW structure for average excitation powers ranging from 0.5 to 2100 μW. Corresponding evolution of (b) the e-h plasma emission intensity integrated between 3.69 and 3.75 eV and (c) emission energy of exciton (X) and biexciton (XX) lines. The dashed-dotted blue line corresponds to the calculated exciton energy by solving the self-consistent Schrödinger-Poisson equation. The vertical dashed line marks the onset of Mott transition corresponding to the red spectrum in (a). See text for details.

excitation power is varied between 0.5 and 2100 μW, corresponding to average power densities ranging between 0.025 and 106 W/cm^2. Considering the duty cycle of the Nd:YAG laser, the peak power is significantly larger than the averaged one and we correspondingly assume that the PL signal is governed by free excitons. The spectra are dominated by the two main emission bands emerging from the QWs, namely, the exciton X at 3.656 eV and the biexciton XX at 3.639 eV. Both emission lines were recently identified in time-resolved experiments[21] and can also be distinguished by the different power law connecting emission intensity and carrier injection. In addition, we can identify the longitudinal optical phonon replica of these transitions located ~92 meV below in energy and the emission of the $Al_{0.2}Ga_{0.8}N$ barrier at 3.775 eV. The power series highlights several interesting features of exciton renormalization. For low excitation densities, only marginal spectral changes can be identified: the exciton undergoes a slight blue-shift <2 meV and gets slightly broader toward the onset of the Mott transition [red spectrum in Fig. 1(a)]. Starting from there, an additional emission band superimposed to the high-energy tail of the exciton appears and rises up. This can also be followed when considering the nonlinear evolution of the integrated PL intensity in this energy range in Fig. 1(b). The appearance of such a high-energy emission band has previously been identified as a trace of an emerging electron-hole plasma recombination in InGaAs/GaAs QWs.[39] Due to the nonidealities of the present experiment, exciton and biexciton emissions remain visible for the whole range of explored power densities. The slight increase in their homogeneous linewidth leads to a vanishing dip between the two emission maxima and slight blue-shifts can be followed up to the highest injection. The latter remains below 3 meV for the exciton. In the end, even when taking into account the integration over inhomogeneously injected QWs in time and depth, an absolute energy shift of the QW exciton exceeding 10 meV up to the Mott density can be ruled out. Neglecting the inhomogeneous vertical carrier injection, and assuming a strict proportionality between excitation power and QW carrier density, and the Mott density given by Eq. (2), i.e., $n_{\mathrm{X}}^{\mathrm{crit}} \sim 1 \times 10^{12}$ cm^{-2},[18] the apparent exciton blue-shift can be solely modeled by the screening of the QCSE [cf. blue line in Fig. 1(c)], while assuming the perfect compensation between BGR and $E_{\mathrm{X}}^{\mathrm{b}}$ reduction for excitons as explained in Sec. III A.

To have a more precise idea of the carrier density impact on the excitonic properties, a homogeneous excitation is required. For this reason, a single GaN/(Al,Ga)N QW was grown with a design close to that of the full MC, i.e., an Al content of 15% and a QW thickness of 2 nm. Figure 2(a) displays a PL power series performed under the same excitation conditions as for the MQW sample at $T = 4$ K. Contrary to the series shown in Fig. 1(a), where both exciton and biexciton transitions dominate the spectra for all excitation densities due to the inhomogeneous vertical injection profile, the e-h plasma emission intensity clearly takes over the exciton one above the Mott transition. Here, the latter is marked by the crossover from a symmetric Voigt-profile-like emission to an asymmetric one [red spectrum in Fig. 2(a)]. This condition is equivalent to the one of a nonlinearly increasing e-h emission intensity such as mentioned before [cf. Figs. 1(b) and 2(b)]. The absence

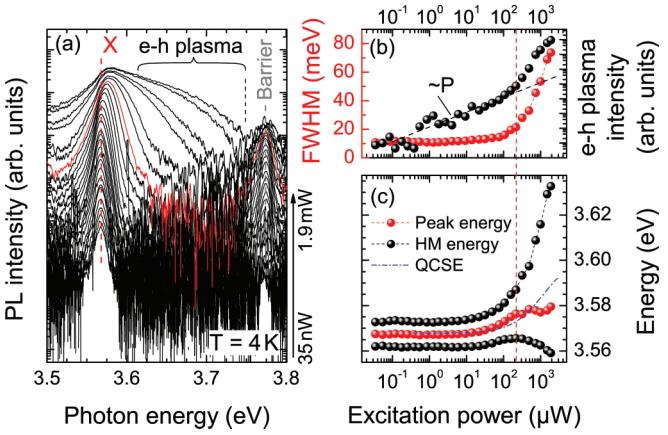

FIG. 2. (Color online) (a) PL power series recorded at 4 K on the GaN/$Al_{0.15}Ga_{0.85}N$ single QW structure for average excitation powers ranging from 0.035 to 1900 μW. Corresponding evolution of (b) QW emission FWHM (red) and the integrated electron-hole plasma emission intensity (black), and (c) peak energy (red), low- and high-energy emission edge (half maximum value: HM). The vertical red dashed line marks the onset of Mott transition corresponding to the red spectrum in (a). The dashed-dotted blue line in (c) corresponds to the calculated exciton energy.

of any biexcitonic signature, probably due to the increased impact of the QCSE,[54] allows monitoring the evolution of the QW-emission full width at half maximum (FWHM). In the low-injection regime, the emission features a narrow linewidth ($\sim$11 meV) and an energy matching the calculated one for the 1s exciton with $E_X^b = 42$ meV. When increasing the carrier density, the FWHM progressively increases up to 20 meV at the Mott transition due to CB. At this point, the line shape gets asymmetric, the high-energy edge of the emission strongly extends and shows a characteristic exponential tail indicating a thermalized e-h population, whereas the low-energy tail follows the band edge and red-shifts due to BGR [cf. Fig. 2(c)]. Furthermore, a blue-shift in the emission maximum can be traced starting from about one order of magnitude below the critical density. It amounts to $\sim$8 meV at the Mott transition. This increased blue-shift value with respect to that observed in the MQW structure highlights on the one hand the concealing effect of an inhomogeneous carrier injection in the MQW structure and on the other hand the increased impact of the QCSE in the single QW.[57] Nevertheless, half of this energy shift can be explained by QCSE screening keeping the same assumptions as before and adopting $n_X^{crit} \sim 7 \times 10^{11}$ cm^{-2} in agreement with Eq. (2). Above n_X^{crit}, the large rise in the FWHM accompanied by the red-shift of the low-energy edge indicates the combined effects of phase-space filling and BGR. Those mechanisms are not considered in the envelope-function calculations for the QCSE screening and manifest themselves only above the Mott density, when the compensation between BGR and E_X^b reduction does not hold anymore, explaining the different evolution of the peak maximum and the simulation.

Conclusively and in agreement with the observations on the MC active medium, an exciton energy shift exceeding 10 meV up to the Mott transition due to the screening of E_X^b can be discarded. No conclusion can be drawn for the evolution of $f_{osc,X}$ from these time-integrated PL measurements. Nevertheless, it is expected that the screening of the QCSE will first lead to a slight enhancement of $f_{osc,X}$ before the vicinity of the Mott transition induces its eventual decrease.

IV. POLARITON RENORMALIZATION: MODELING VERSUS EXPERIMENT

A. Modeling

The dispersion of exciton polaritons in a planar MC is often simply modeled by considering the eigenmode spectrum of two coupled oscillators, namely, the photonic $E_C(k_\parallel)$ and excitonic $E_X(k_\parallel)$ modes, featuring a certain interaction constant g. Although this treatment corresponds to a rather crude approximation neglecting the dispersion of the refractive index, any inhomogeneous linewidth contribution, the impact of the electron-hole continuum absorption and potential modifications of the optical confinement with changing photon energy and increasing external angle, its ease of use, and the good agreement observed with experiments justifies its application. The matrix representation of the system Hamiltonian in the basis of the uncoupled modes for a single exciton is given by

$$\begin{pmatrix} E_X(k_\parallel) - i\gamma_X & g \\ g & E_C(k_\parallel) - i\gamma_C \end{pmatrix}. \quad (7)$$

Figure 3(a) shows the eigenmode spectrum using realistic values for the current MC structure at room temperature (cf. Fig. 4), namely, an exciton with energy $E_X = 3.631$ eV and homogeneous linewidth $\gamma_X = 25$ meV, a small negative exciton-cavity photon detuning $\delta = -15$ meV, a cavity mode with effective refractive index $n_C = 2.65$ and linewidth

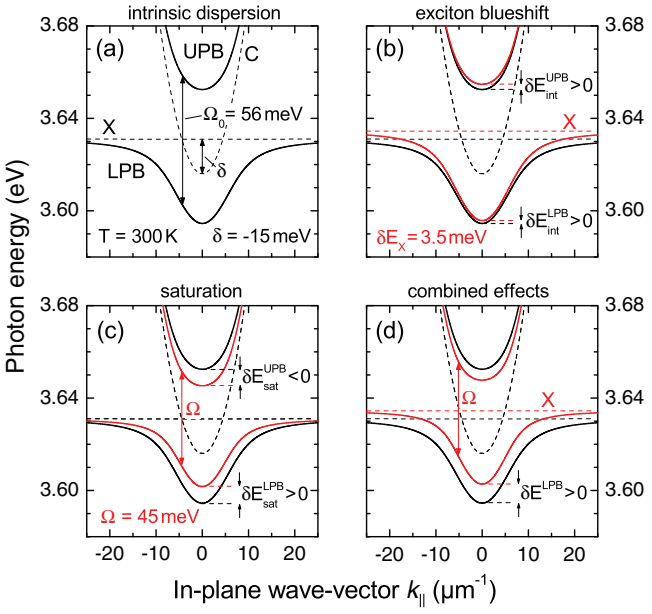

FIG. 3. (Color online) (a) Intrinsic polariton dispersion (black lines) corresponding to the MQW-based MC investigated in this work for $\delta = -15$ meV at room temperature. Renormalized polariton dispersion (red lines) due to (b) exciton-exciton interaction (exciton blue-shift), (c) $f_{osc,X}$ saturation, and (d) the combined effects. The bare modes, excitons (X), and cavity photons (C) are shown with dashed lines.

$\gamma_C = 4$ meV, and a zero-density coupling strength $g_0 = g(n_X = 0) = 30$ meV.[18] The uncoupled modes split up into the lower and upper polariton branches (LPB and UPB), which exhibit a minimum initial energy splitting $\Omega_0 = 56$ meV. This value is reduced with respect to the doubled value of g_0 owing to the influence of the finite linewidths of the modes.

When increasing the carrier injection, any modification in the excitonic optical response according to Eq. (3) will directly induce a renormalization of the polariton dispersion:

$$E_{\mathrm{LPB},0} \rightarrow E_{\mathrm{LPB}} \quad \text{and} \quad E_{\mathrm{UPB},0} \rightarrow E_{\mathrm{UPB}}.$$

Figure 3(b) depicts the impact of a changing exciton energy according to Eq. (4). Given that the cavity mode remains unaffected,[58] this modification simply corresponds to a change in detuning δ. Both polariton branches are displaced by the exciton blue-shift, which in this case is assumed to amount to 3.5 meV, multiplied with their excitonic fraction $|X_{k_\parallel}|^2$ defined by

$$\left|X_{k_\parallel}\right|^2 = \Omega^2/\left(\Omega^2 + 4\left[E_{\mathrm{LPB}}(k_\parallel) - E_X(k_\parallel)\right]^2\right). \tag{8}$$

The Hopfield coefficients are connected via the unitary relation $|X_{k_\parallel}|^2 + |C_{k_\parallel}|^2 = 1$, where $|C_{k_\parallel}|^2$ denotes the photonic fraction. For negative detunings, this only results in a marginal shift around zero in-plane momentum for the LPB, while the high-angle regions are strongly affected.

The behavior is different when an increasing γ_X or a decreasing $f_{\mathrm{osc,X}}$ are considered. While the uncoupled modes remain unchanged, the polariton dispersions feature a decreasing Rabi splitting: $\Omega_0 \rightarrow \Omega$. In the case of γ_X, this directly results from the eigenvalue problem of Eq. (7), while for a changing $f_{\mathrm{osc,X}}$ the coupling constant is modified. Presuming a QW-based MC, where the overlap between the electric cavity field and the excitonic wave function is independent of injection, $f_{\mathrm{osc,X}}$ will directly influence the coupling strength via[60,61]

$$g = \hbar\sqrt{\frac{e^2}{2\varepsilon_0 m_0}\frac{N_{\mathrm{QW}}^{\mathrm{eff}}}{n_C^2 L_{\mathrm{eff}}} f_{\mathrm{osc,X}}}, \tag{9}$$

where e, m_0, and $\hbar$ denote the electron charge, its free mass, and the reduced Planck constant, respectively. Apart from $f_{\mathrm{osc,X}}$, g only depends on structure-dependent properties, namely n_C, the number of effectively coupled QWs $N_{\mathrm{QW}}^{\mathrm{eff}}$, and finally the effective cavity length L_{eff} such as defined in Ref. 61. Figure 3(c) shows the effect of a Rabi-splitting decrease down to 45 meV, which could be either caused by an increased exciton linewidth of $\gamma_X = 44$ meV or a reduction in $f_{\mathrm{osc,X}}$ by 30%. Contrary to the change induced by interaction, saturation leads to oppositely shifting branches: While the LPB is still blue-shifting, the UPB undergoes a red-shift. Thereby, the amount of the shift depends on the in-plane wave-vector-dependent detuning. It is larger for small energy splittings.

Finally, the combined impact of both effects is shown in Fig. 3(d). Interestingly, the energy shift of the LPB looks quasirigid, i.e., whatever the in-plane wave vector the summed contribution of interaction and saturation provides a comparable energy renormalization. This finding does certainly depend on the respective weights of the two contributing effects and the detuning, but it highlights their different impact and agrees well with previous experimental results obtained on this MC structure.[16] Conclusively, in this coupled-oscillator model (COM), the evolution of the polariton ground-state energy shift $\delta E_0 = E_{\mathrm{LPB}}(k_\parallel = 0) - E_{\mathrm{LPB},0}(k_\parallel = 0)$ is issued from two contributions: (i) the saturation $\delta E_0^{\mathrm{sat}}$, i.e., a change in the Rabi splitting $\delta\Omega$, and (ii) pure Coulomb interaction $\delta E_0^{\mathrm{int}}$. A simple linear expansion in δE_X and $\delta\Omega$ leads to

$$\delta E_0^{\mathrm{int}}(n_X) \sim |X_{k_\parallel}|^2 \delta E_X(n_X), \tag{10}$$

$$\delta E_0^{\mathrm{sat}}(n_X) \sim \frac{\Omega_0}{2\sqrt{\delta^2 + \Omega_0^2}}\delta\Omega(n_X). \tag{11}$$

Despite the idealization of the structure, the COM appears convenient for the description of the linear regime where no distinction is made between the contribution of the excitonic reservoir and the polariton ground-state population to the LPB renormalization. Indeed, below threshold, the ground-state occupancy is negligible and the renormalization is mainly governed by the reservoir, whereas above threshold the large condensate population drastically impacts on the ground-state renormalization and should be properly taken into account. In the mean-field approximation,[62] and following the semiclassical Boltzmann formalism,[63] it was found that above the condensation threshold, the reservoir population is clamped to its threshold value n_{thr}, while the condensate density n_0 grows linearly with the injected carrier density, i.e., $n_0 \propto (n_X - n_{\mathrm{thr}})/\gamma_C$. This is a situation similar to that occurring in semiconductor laser diodes when considering the electron-hole plasma population and the density of photons of stimulated origin.

B. Experimental results

In the following section, we will focus on the emission properties of the full MC operating in the SCR. Keeping in mind the extensive range of accessible negative detunings in the present MC structure, the analysis of the far-field emission promises a deep insight into the renormalization process as both very photonlike states at the bottom of the LPB and very excitonlike ones at higher emission angles can be tracked simultaneously. In this way, effects associated to an exciton energy shift or a decrease in the light-matter coupling strength can be easily separated. In Figs. 4(a)–4(c) and 4(e)–4(g), Fourier images are reported for two power series up to the condensation threshold corresponding to different detuning and lattice temperature combinations (δ, T), namely, (−5 meV,40 K) and (−54 meV,280 K). These two series are representatives of a set of measurements exhibiting a very similar behavior. Solely the LPB is observed in PL measurements, which is due to an efficient carrier relaxation, residual absorption within the cavity, and a low thermal occupancy of the UPB. The LPB exhibits a pronounced blue-shift with increasing power density, visible in particular around $k_\parallel = 0$. The branch evolution has been analyzed within the previously described COM. A satisfactory reproduction of the dispersion over the full power range is only achieved when introducing a decreasing Rabi splitting. Due to the relative constancy of the LPB emission energy at higher angles with increasing injection, a large blue-shift of the QW resonance can be excluded in agreement with the experimental findings shown in

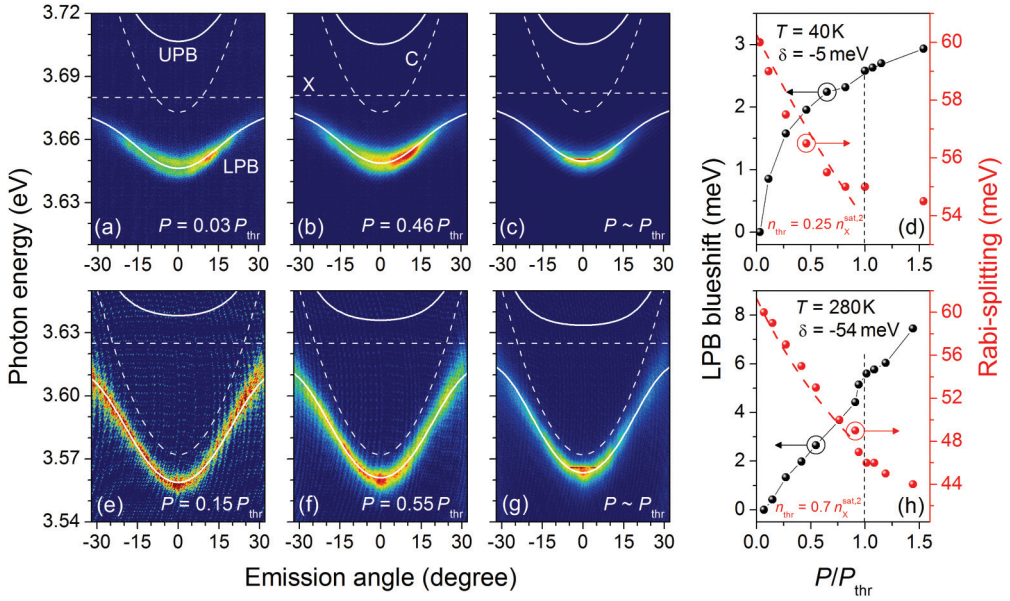

FIG. 4. (Color online) Far-field emission pattern of the full MC measured under nonresonant pulsed excitation at (a)–(c) 40 K for $\delta = -5$ meV and (e)–(g) 280 K for $\delta = -54$ meV for various excitation power densities. The bare modes X and C are shown with white dashed lines and the polariton branches with white continuous lines. Figures (d) and (h) display the power evolution of the LPB blue-shift and the Rabi splitting for each situation. The red dashed lines reproduce the expected Ω reduction from the COM and account for the different carrier densities at threshold.

Sec. III C. Moreover, when considering the 280-K series shown in Figs. 4(e)–4(g), an explanation for the observed blue-shift of ∼6 meV up to threshold only based on interactions according to Eq. (10), and adopting an excitonic fraction of 18%, would require an exciton blue-shift exceeding 30 meV. This represents a clear contradiction with the experiment. In order to address the respective weights of CB and $f_{\mathrm{osc,X}}$ saturation, the LPB linewidth γ_{LPB} shall be investigated. For the 40-K series at $k_{\parallel}=0$, no significant changes in γ_{LPB} can be identified up to the polariton lasing threshold, as confirmed by its constant value equal to (10 ± 0.5) meV. A slightly different behavior can be tracked for the high-temperature series. Here, it is useful to examine γ_{LPB} at high external angles due to an increased excitonic fraction. At 30° the linewidth increases from 16 to 19 meV at threshold. According to Eq. (7) and considering the local Q factor (∼600), a slight increase in the exciton homogeneous linewidth of 5 meV can be deduced from the COM. Such moderate, or in the case of the 40-K series even negligible, values are in good agreement with the experimental results shown in Fig. 1 and can only explain a Ω reduction of about 1 meV. By process of elimination, $f_{\mathrm{osc,X}}$ saturation is thus found to be the dominant polariton-renormalization mechanism in the present MC structure. Note further that the polariton energy at $k_{\parallel}=0$ remains below the cavity mode energy over the whole power range investigated, ensuring that the SCR is preserved. Another interesting aspect is that the decrease in Ω significantly slows down once the condensation threshold is crossed. This feature indicates that renormalization is mainly set by the exciton reservoir whose density is expected to be clamped above the condensation threshold.[62,63] Similar effects have been observed in a nonpolar GaN MQW-based MC.[64]

Owing to the significant in-plane disorder, of both excitonic and photonic origin, the presence of QWs apart from the cavity antinodes, and other nonidealities in the structure, part of the oscillator strength is transferred from the system bright states, i.e., the LPB and UPB, to so-called dark exciton states.[21] This property allows probing excitonic features by means of PL measurements in the full MC. Note that even if this excitonic signal mainly originates from uncoupled QWs, it still gives access to the exciton renormalization inside the MC. Considering a laser penetration depth in the cavity of ∼100 nm, most of the carriers are created within the first 10–15 QWs. After relaxation, radiative excitons are redistributed in the whole cavity section due to Rabi oscillations. Dark excitons, being either uncoupled from the cavity mode or dark by their spin projection, do not participate in the light-matter interaction. They possess a long lifetime and remain distributed according to the pump absorption profile. Thus, their PL signal mostly stems from highly injected QWs.

In Fig. 5(a), the PL far field of the MC structure at moderate injection is displayed up to high angles (>50°) at 10 K. Aside from the strong LPB emission showing a clear inflection point, PL signatures of the dark excitons and biexcitons are visible. Both modes have been identified in a previous study.[21] In Fig. 5(b), the spectral profiles at $k_{\parallel}=0$ of a power series performed at the same sample spot reveal no significant modification in the dark exciton PL signal over the full injection range explored up to $3.22\,P_{\mathrm{thr}}$. After careful deconvolution, the energy shift of the free exciton at $k_{\parallel}=0$ is found to be lower than 1 meV up to the highest carrier density probed in perfect agreement with the findings on the bare active medium given in Sec. III C. In addition, the high-energy side of the emission does not show any variation with injection [cf.

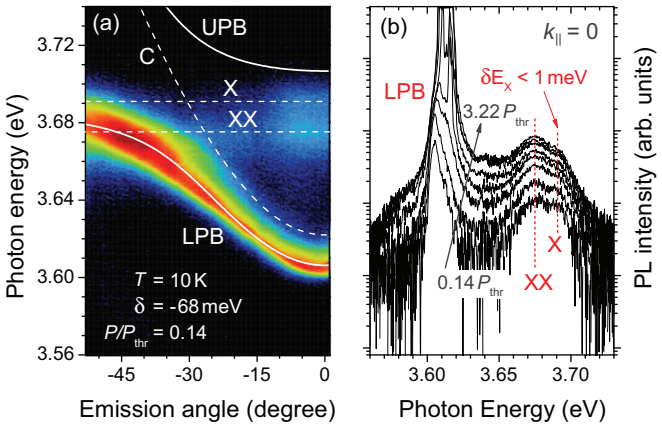

FIG. 5. (Color online) (a) Far-field emission pattern of the full MC ($\lambda_{exc} = 266$ nm) measured at 10 K for $\delta = -68$ meV below the condensation threshold. The bare modes, i.e., X, C, and XX are shown with white dashed lines and the polariton branches are shown with white continuous lines. (b) Spectral profiles at $k_{\parallel} = 0$ obtained at the same position with identical excitation conditions for a varying injection ranging from 0.14 to $3.22P_{thr}$. The position of X and XX lines is highlighted with red dashed lines.

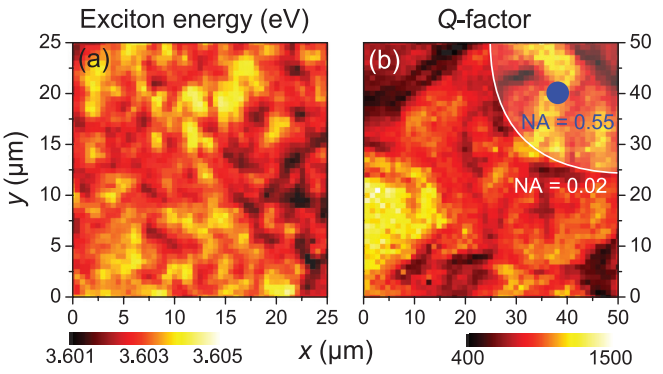

FIG. 6. (Color online) (a) Excitonic and (b) photonic disorder mappings measured at $T = 300$ K. The blue and white circles represent the approximative excitation spot size when either the microscope objective (NA = 0.55) or a conventional lens (NA = 0.02) is used. Note the different spatial scales for the two mappings.

Fig. 1(a)], which indicates that the system still operates below the Mott transition and confirms a marginal impact of CB.

Eventually, in agreement with previous findings shown in Ref. 16, the dominating renormalization effect appears to be a decreasing Rabi splitting and only small exciton blue-shifts $\delta E_X \leqslant 3$ meV are observed [cf. Figs. 4(a)–4(c), and 5(b)]. This assumption is further confirmed when evaluating the ratio of each contribution $\delta E_0^{int}/\delta E_0^{sat}$ with relations (10) and (11): for the whole (δ,T) range considered in this work, the impact of interaction remains below 10%. Even when completely neglecting any excitonic shift and the impact of CB, the behavior of Ω can be successfully reproduced with Eqs. (6) and (9), the exciton density at threshold n_{thr} being the unique adjustable parameter [red dashed lines in Figs. 4(d) and 4(h)]. Note that in both cases, n_{thr} lies below but close to $n_X^{sat,2}$ ($0.25n_X^{sat,2}$ and $0.7n_X^{sat,2}$, respectively). The final value of $\delta\Omega$ is then only conditioned by the relative carrier density at threshold $n_{thr}/n_X^{sat,2}$, which in turn essentially depends on the combination of δ and T as revealed by previous studies [cf. Fig. 7(b)].[16,19] In particular, it was seen that for each lattice temperature, an optimum detuning δ_{opt} exists at which n_{thr} is minimized. Contrary to vertical-cavity surface-emitting lasers, δ_{opt} is a nontrivial function of temperature and depends on the interplay between kinetics and thermodynamics. For the present MC, δ_{opt} continuously shifts toward negative values when T is increased, highlighting the predominant role of thermodynamics in our system. This trend is accelerated for $T > 200$ K, where thermal depopulation of the ground state is activated. This extra source of loss inhibits the formation of the polariton condensate and is more efficient at more positive detunings where the trap formed by the LPB is shallower.[19,65]

In order to further confirm the role of the phase diagram on the polariton renormalization, the LPB blue-shift at $k_{\parallel} = 0$, δE_0, has been measured for different (δ,T) combinations using Fourier imaging. Surprisingly, the results are extremely scattered (not shown here) evidencing no clear correlation between $\delta E_0(\delta,T)$ and the n_{thr} value predicted by the phase diagram. In order to understand this behavior, the impact of photonic and excitonic disorder has to be considered, as they play an important role in III-nitride based MCs.[66,67] In Fig. 6(a), the spatial mapping of the exciton energy measured on the bare active region is shown. It exhibits a mean energy fluctuation of 2–3 meV at a spatial scale smaller than the spot size used for Fourier imaging. With respect to γ_X^{inh} and the large detuning range explored, only a marginal effect of excitonic disorder on the polariton renormalization is thus expected. A different conclusion can be drawn for the photonic disorder displayed by a mapping of the local Q factor of the full MC in Fig. 6(b).[68] Its fluctuation scale approximately corresponds to that of the Fourier-imaging laser spot size. The relatively large variations in the Q values, ranging from 400 to 1500, have a strong impact on the condensation threshold as they directly affect the polariton lifetime. Since any change in the system dynamics leads to variations in the imbalance between kinetics and thermodynamics, n_{thr} will fluctuate at the same lateral scale.

For the purpose of eliminating the unpredictable contribution of in-plane static disorder on the polariton renormalization, the $\delta E_0(\delta,T)$ study has been repeated with a larger spot size [NA = 0.02, cf. white circle in Fig. 6(b)]. The exciton and cavity energies are now averaged over a region of 50-μm diameter, resulting in well-defined values for the exciton and photon energies, but with a larger inhomogeneous broadening. Averaging over the photonic disorder results in a mean Q factor of about 1000 which is in perfect agreement with the value reported for the present sample in a comparable configuration.[18]

Figure 7(a) displays the blue-shift of the polariton ground-state energy at threshold as a function of δ and T using a larger spot size. Contrary to the above-mentioned micro-PL study, some correlations now become visible. For $T \leqslant 100$ K, the experimental results exhibit a remarkable independence on δ. On the contrary, for $T = 300$ K the blue-shift is strongly increasing toward positive detuning, while for $T = 200$ K an intermediate situation is recorded. With rising temperature, an overall increase in the blue-shift is observed, whereas the variation below 200 K remains very weak.

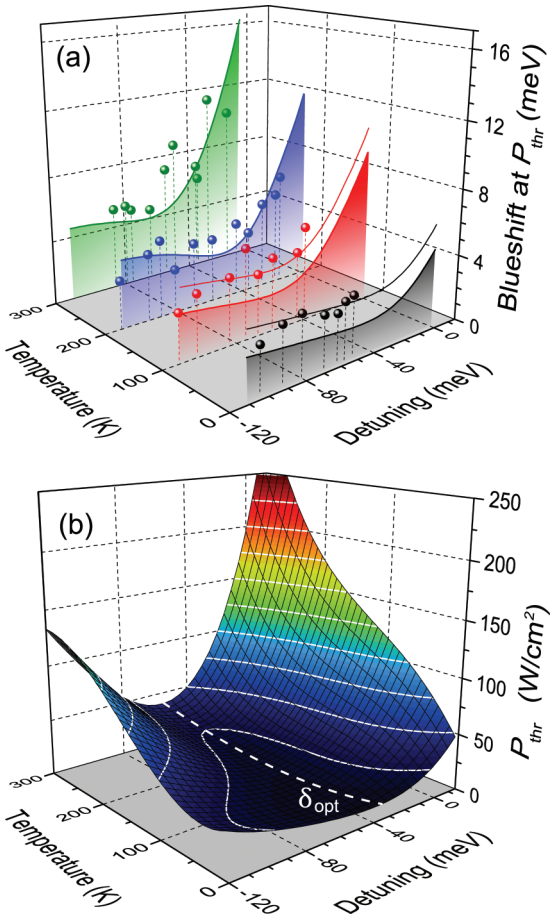

FIG. 7. (Color online) (a) Mapping of the blue-shift of the polariton ground state measured at $P = P_{\rm thr}$ as a function of T and δ: comparison of modeling (continuous lines) and experiment (dots). For $T \leqslant 100$ K, artificially upshifted (by 1.5 meV) modeling curves are added to account for the highly nonlinear blue-shift mechanism present at low temperatures. (b) Dependence of the polariton lasing threshold power density on T and δ represented by a polynomial fit of the experimental data from Ref. 16.

In order to reproduce the behavior of $\delta E_0(\delta, T, n = n_{\rm thr})$, simulations using the COM were performed accounting for $f_{\rm osc,X}$ saturation and the correction of $n_{\rm thr}$ given by the phase diagram in Fig. 7(b).[69] Below the condensation threshold, most of injected carriers populate the excitonic reservoir and the LPB occupancy is conditioned by the relaxation efficiency. Thus, the overall carrier lifetime is close to the one of the free exciton,[21] and for a given temperature one can reasonably assume $n_{\rm X}/n_{\rm thr} \propto P/P_{\rm thr}$, where P is the pump power density measured experimentally. Note that this ratio might be changing with temperature due to variations in the carrier lifetime, the internal quantum efficiency, and carrier localization and delocalization effects. However, in line with the treatment shown in Ref. 19, these complex effects have been neglected as a first approximation, leading to the ratio n/P as being the only adjustable scaling parameter fixed by $P(n_{\rm X}^{\rm sat,2}) = 65$ W/cm^2. The result of the COM simulations is shown by the down-projected solid lines in Fig. 7(a). Apart from the global trend of an increasing blue-shift with temperature for a given δ, which is a result of the rising thermodynamic threshold of the system,[19] a strong rise in the expected blue-shift toward positive δ values is obvious. Whereas it is absent in the experimental data for low temperatures, due to the inaccessibility of corresponding δ values, a very good agreement between experiment and modeling is reached for $T \geqslant 200$ K. Two different effects contribute here: First, for a $\delta(k_\parallel)$ close to zero and thus a large splitting between bare and coupled modes, the renormalization due to saturation is stronger (cf. Sec. IV A). Second, for higher temperatures, thermal escape of polaritons from the bottom of the LPB trap increases the condensation threshold density.[16,19] For more negative δ values, the behavior of δE_0 is rather intricate as it is driven by two opposite contributions. On the one side, the blue-shift induced by $f_{\rm osc,X}$ saturation decreases due to the proximity of the cavity mode and on the other side the large rise in $n_{\rm thr}$ for negative detunings due to the carrier kinetics limitation should result in an increase in δE_0. For an intermediate δ range, both effects partly compensate each other explaining the experimentally observed δ independence. For even more negative detuning (beyond the explored δ range), the LPB renormalization would become completely negligible due to the disappearance of the excitonic character and δE_0 would tend to zero: this is the pure photonic case.

Whereas experimental data are well reproduced for $T \geqslant 200$ K, the blue-shifts at lower lattice temperature only follow qualitatively the expected detuning dependence, but are upshifted by about 1.5 meV compared to the expectations. In order to properly comment this feature, the density-dependent evolution of the polariton ground-state energy $\delta E_0(n_{\rm X})$ for given δ and T values, corresponding to different points displayed in Fig. 7(a), shall be considered in the following. In Fig. 8, the blue-shift of the LPB at $k_\parallel = 0$ is displayed as a function of normalized pump power for a constant detuning of about -60 meV for four different lattice temperatures ranging between 10 and 300 K. As renormalization is dominated by saturation effects and no significant change in the n/P ratio

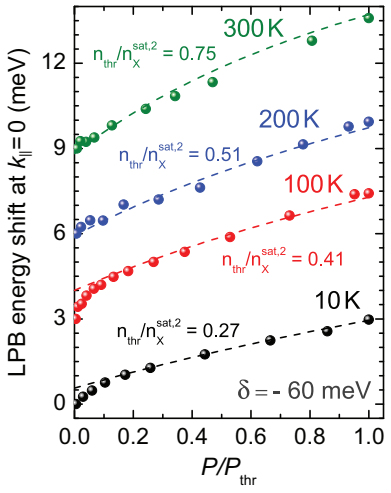

FIG. 8. (Color online) Evolution of the polariton ground-state energy vs normalized pump power density $P/P_{\rm thr}$ for different lattice temperatures ranging between 10 and 300 K for $\delta \approx -60$ meV. The dashed lines correspond to fits accounting for the phase diagram and saturation of $f_{\rm osc,X}$ in the COM. High-temperature data have been shifted vertically with respect to the 10-K case for clarity.

is expected, $\delta E_0(n_X)$ should be well described by Eq. (11) for all power series whatever the detuning and temperature. Each curve has been fitted correspondingly by scaling only the relative power density at threshold $n_{thr}/n_X^{sat,2}$. In agreement with our assumption, the values deduced for $n_{thr}/n_X^{sat,2}$ remain below the critical value. They rise with lattice temperature and nicely match the threshold values extracted from the phase diagram.[16,19] For $T_{lat} \geqslant 200$ K, the evolution of the ground-state energy including the slight sublinear scaling is adequately reproduced by considering saturation effects only. By contrast, for lower lattice temperatures, a clear deviation from the expected behavior is observed. In the low injection regime, i.e., for $P/P_{thr} \leqslant 0.15$, an additional nonlinear blue-shift mechanism is revealed, which is present for $T_{lat} \leqslant 100$ K whatever the probed region, spot size, and detuning. This effect is also apparent in the power series of Figs. 4(a)–4(d). Whereas for each injection the LPB dispersion is well fitted by an almost constant exciton energy and a Rabi splitting decreasing with rising excitation power, the evolution of the coupling strength with excitation power itself is rather poorly reproduced by the assumed $f_{osc,X}$ scaling [cf. Eq. (6) and red dashed line in Fig. 4(d)]. Since neither $f_{osc,X}$ saturation nor the influence of CB can serve as possible origin for this additional blue-shift mechanism,[70] a physical interpretation of the latter lies beyond the scope of the current modeling. It might thus lead to an overestimate of the $n_{thr}/n_X^{sat,2}$ ratio for $T_{lat} \leqslant 100$ K and explain the static offset between modeling and experiment visible in Fig. 7(a). Its possible origin shall now be discussed briefly.

Note that the applied modeling neglects any variation in the n/P ratio with lattice temperature and carrier density and represents thus a rather crude approximation. Owing to localization effects occurring at low temperatures, the effective carrier lifetime might be noticeably longer, leading automatically to a larger n/P ratio. In agreement with the QW-exciton localization energy $E_X^{loc} \sim 11$ meV,[21] such a mechanism could explain the energetic offset at low temperatures seen in Fig. 7(a) and potentially also the blue-shift nonlinearity observed at low injection in Fig. 8 when supposing that carrier delocalization occurs exactly in this excitation regime. Indeed, with increasing injection, the localization might be lifted and both the carrier lifetime as well as the n/P ratio would decrease, resulting in a decreasing blue-shift rate at those carrier densities. Another mechanism related to carrier localization effects was discussed by Rhee *et al.*:[51] Carrier scattering occurring on the local disorder landscape could lead to a population transfer between radiative and nonradiative states and would also strongly impact on the light-matter coupling strength. However, in a MC exciton localization effects are usually supposed to play a negligible role, as at least for radiative excitons localization is prevented by ultrafast Rabi oscillations and the contribution of localized states to the strong light-matter interaction is ruled out by their low density of states. Moreover, when considering the absence of any signature of delocalization like a characteristic *s*-shaped exciton blue-shift at low densities in the power series of Fig. 1, carrier localization effects as possible origin should at least be put into question, even though this mechanism seems likely.

An alternative explanation for the discrepancy existing between modeling and experiment could be given by cavity biexcitons: In a recent work, it has been demonstrated that biexcitons participate in the formation of polariton condensates.[21] Indeed, the impact of a biexciton-mediated interaction is supposed to result in an effective polariton-polariton attraction scaling nonlinearly with carrier density.[7,71] Even the observed restriction to low temperatures appears to be consistent with the thermal dissociation of biexcitons occurring around 200 K in the present MQW structure. However, theoretical investigations only involve virtual scattering states, thus partly relieving the temperature argument, and the constraint to very low power densities contradicts any expected biexciton power law, eventually making this effect very unlikely.

Conclusively, on the basis of the present measurements, it is too premature to unambiguously conclude on the exact mechanism governing the polariton renormalization in this temperature and density range. Carrier localization effects appear to be the most likely reason, but the exact mechanism at play remains ultimately an open question.

V. DISCUSSION AND OUTLOOK

It is worth pointing out that the relations given here to describe the effect of exciton saturation via an absolute particle density are based on theoretical models only and require an experimental verification. In particular, the ratio between n_X^{crit} and $n_X^{sat,2}$ remains an open question. The first quantity embodies the transition between an exciton gas and an uncoupled electron-hole plasma, whereas $n_X^{sat,2}$ only defines the density where $f_{osc,X}$ is halved. A connection between them stays beyond the reach of the current experiments. Whereas the studies on the QWs exclusively dealt with n_X^{crit} preventing any inference on the $f_{osc,X}$ evolution, the experimental analysis on the MC only depends on $n_X^{sat,2}$, as long as $n_X^{crit} \geqslant n_X^{sat,2}$. Nevertheless, the presence of a finite Rabi splitting at the condensation threshold and above ensures that the system operates well below the Bernard-Duraffourg limit, likely up to two orders of magnitude below depending on the ratio $n_X^{crit}/n_X^{sat,2}$ and the (δ,T) combination.

In the end, a clear understanding of the renormalization mechanisms is important for achieving an accurate description of polariton fluids. In particular, when evaluating absolute condensate carrier densities or simulating polariton nonlinearities using the Gross-Pitaevskii equation, it is frequently assumed that saturation effects play a marginal role.[8,13] This is usually justified by an earlier theoretical work,[44] where the ratio between saturation and interaction contributions to polariton renormalization should only depend on scalable material and sample parameters, namely, $(\Omega/E_X^b)^2$. This relation does not accurately apply to realistic systems as it is derived for zero temperature and shows no strong density dependence. Moreover, for recent high-quality MCs based on different material systems, the corresponding fraction appears to be significant (cf. Table I), which is in agreement with various experimental observations. Low-temperature studies have clearly established the increasing role of saturation effects on the polariton states in both GaAs (Refs. 30 and 51) and CdTe (Ref. 72) MC systems, when the carrier density is raised starting approximately one order of magnitude below the saturation one. Although those experiments have been led

TABLE I. Theoretical impact of saturation for MCs based on different material systems following Ref. 44.

Material system	GaAs	CdTe	GaN	ZnO	Anthracene
Reference	73	2	17	9	74
$(\Omega/E_X^b)^2$	0.22	0.087	0.093	0.29	<0.01

on MCs, which do not exhibit a nonlinear polariton emission, the recorded relative proximity between polariton and photon lasing thresholds in high-quality GaAs-based MCs (Ref. 73) suggests a general operation of polariton lasers only one or two orders of magnitude below n_X^{crit}. Thus, a pronounced impact of saturation effects is expected whatever the material system. This is in agreement with the experimental findings of this work, and with other experimental results, where a red-shifting UPB was observed in PL,[2,16] or a decreasing Rabi splitting has been recorded.[64] In order to demonstrate this impact, we would like to stress the fact that even a moderate renormalization scenario of the polariton branch at threshold like in the power series of Figs. 4(e)–4(h) leads to a change in the effective polariton mass of about 5%. Such a modification should be carefully taken into account, for instance, when investigating the flow of polaritons away from their excitation spot and related effects.[14,15] In this case, the effective polariton mass will become strongly spatially, density, and time dependent, which could have profound consequences for the physics of polariton fluids. It is worth mentioning that MCs based on organic semiconductors as an active medium should be excluded from the conclusion of a pronounced saturation impact. Here, the giant binding energy of Frenkel excitons pushes the saturation density to much higher values in agreement with the absence of any significant LPB blue-shift in experiments.[75]

Note finally that the analysis drawn in this paper is exclusively valid below the polariton condensation threshold. When crossing the latter, the significant photonic disorder present in GaN-based MCs creates traps for polariton condensates, which usually results in a strong discontinuity in δE_0 and the onset of multimode emission. Both effects make a comprehensive discussion even more complex. While polariton renormalization is primarily governed by the exciton reservoir below the condensation threshold, above the latter the interactions occurring in the condensate and the unknown impact of the condensate population on the exciton saturation might alter the characteristics. Irrespective of the impact of a changing mean-particle lifetime, hints for this are given by a change in the LPB blue-shift power law across the threshold,[13,76] or by the observed slowdown of the Rabi decrease in this work and in Ref. 64.

VI. CONCLUSION

It has been shown that for III-nitride based MCs, polariton renormalization is primarily governed by exciton saturation effects, while the influence of excitonic blue-shift was found to be marginal. Evidences were found in the absence of any significant exciton energy shift in (i) the optically induced Mott transition in bare GaN/AlGaN QWs, (ii) the LPB dispersion of injection-dependent Fourier-imaging series, and (iii) the emission of dark exciton states across the condensation threshold in the full MC. Note that in the present MC system, this influence might even be overestimated due to QCSE screening, which is absent in GaAs or CdTe systems. Moreover, a pronounced correlation of the saturation impact with detuning and temperature was tracked, which is arising from the opposite influence of different mechanisms. As shown by simulations, saturation is expected to be stronger for large splittings between bare and polariton modes, i.e., for a detuning close to zero. This effect superimposes on the polariton condensation phase diagram, i.e., on the dependence of the polariton lasing threshold on detuning and temperature, and thus on the vicinity between this latter threshold and the exciton saturation density.[16,19] As far as the transferability of the present results to other systems is concerned, the similar behavior observed for highly injected GaAs QWs,[39] and the comparable proximity of the polariton lasing threshold and Mott transition in GaAs-based MC systems,[73] means that a pronounced impact of saturation effects can be expected for all inorganic MC material systems.

ACKNOWLEDGMENT

This work was supported by the NCCR Quantum Photonics, research instrument of the Swiss National Science Foundation (SNSF), by the SNSF (Grant No. 200020-113542), and by the EU-project Clermont4 (Grant No. FP7-235114).

*georg.rossbach@epfl.ch
†Now at Novagan S.a.r.l., Chemin de Mornex 5, CH-1003 Lausanne, Switzerland.

[1] L. S. Dang, D. Heger, R. André, F. Bœuf, and R. Romestain, Phys. Rev. Lett. **81**, 3920 (1998).
[2] J. Kasprzak, M. Richard, S. Kundermann, A. Baas, P. Jeambrun, J. M. J. Keeling, F. M. Marchetti, M. H. Szymanska, R. André, J.-L. Staehli, V. Savona, P. B. Littlewood, B. Deveaud-Plédran, and L. S. Dang, Nature (London) **443**, 409 (2006).
[3] R. Balili, V. Hartwell, D. Snoke, L. Pfeiffer, and K. West, Science **316**, 1007 (2007).
[4] S. Christopoulos, G. Baldassarri Höger von Högersthal, A. J. D. Grundy, P. G. Lagoudakis, A. V. Kavokin, J. J. Baumberg, G. Christmann, R. Butté, E. Feltin, J.-F. Carlin, and N. Grandjean, Phys. Rev. Lett. **98**, 126405 (2007).
[5] F. Tassone, C. Piermarocchi, V. Savona, A. Quattropani, and P. Schwendimann, Phys. Rev. B **56**, 7554 (1997).
[6] S. Schmitt-Rink, D. S. Chemla, and D. A. B. Miller, Phys. Rev. B **32**, 6601 (1985).
[7] M. Vladimirova, S. Cronenberger, D. Scalbert, K. V. Kavokin, A. Miard, A. Lemaître, J. Bloch, D. D. Solnyshkov, G. Malpuech, and A. V. Kavokin, Phys. Rev. B **82**, 075301 (2010).

[8]M. Richard, J. Kasprzak, R. André, R. Romestain, L. S. Dang, G. Malpuech, and A. V. Kavokin, Phys. Rev. B **72**, 201301 (2005).
[9]T. Guillet, M. Mexis, J. Levrat, G. Rossbach, C. Brimont, T. Bretagnon, B. Gil, R. Butté, N. Grandjean, L. Orosz, F. Réveret, J. Leymarie, J. Zúniga-Pérez, M. Leroux, F. Semond, and S. Bouchoule, Appl. Phys. Lett. **99**, 161104 (2011).
[10]H. Franke, C. Sturm, R. Schmidt-Grund, G. Wagner, and M. Grundmann, New J. Phys. **14**, 013037 (2012).
[11]K. Sebald, M. Seyfried, S. Klembt, S. Bley, A. Rosenauer, D. Hommel, and C. Kruse, Appl. Phys. Lett. **100**, 161104 (2012).
[12]C. Ciuti, P. Schwendimann, B. Deveaud, and A. Quattropani, Phys. Rev. B **62**, R4825 (2000).
[13]L. Ferrier, E. Wertz, R. Johne, D. D. Solnyshkov, P. Senellart, I. Sagnes, A. Lemaître, G. Malpuech, and J. Bloch, Phys. Rev. Lett. **106**, 126401 (2011).
[14]G. Christmann, G. Tosi, N. G. Berloff, P. Tsotsis, P. S. Eldridge, Z. Hatzopoulos, P. G. Savvidis, and J. J. Baumberg, Phys. Rev. B **85**, 235303 (2012).
[15]A. Amo, J. Lefrère, S. Pigeon, C. Adrados, C. Ciuti, I. Carusotto, R. Houdré, E. Giacobino, and A. Bramati, Nat. Phys. **5**, 805 (2009).
[16]R. Butté, J. Levrat, G. Christmann, E. Feltin, J.-F. Carlin, and N. Grandjean, Phys. Rev. B **80**, 233301 (2009).
[17]G. Christmann, R. Butté, E. Feltin, J.-F. Carlin, and N. Grandjean, Appl. Phys. Lett. **93**, 051102 (2008).
[18]G. Christmann, R. Butté, E. Feltin, A. Mouti, P. A. Stadelmann, A. Castiglia, J.-F. Carlin, and N. Grandjean, Phys. Rev. B **77**, 085310 (2008).
[19]J. Levrat, R. Butté, E. Feltin, J.-F. Carlin, N. Grandjean, D. Solnyshkov, and G. Malpuech, Phys. Rev. B **81**, 125305 (2010).
[20]J. Levrat, R. Butté, T. Christian, M. Glauser, E. Feltin, J.-F. Carlin, N. Grandjean, D. Read, A. V. Kavokin, and Y. G. Rubo, Phys. Rev. Lett. **104**, 166402 (2010).
[21]P. Corfdir, J. Levrat, G. Rossbach, R. Butté, E. Feltin, J.-F. Carlin, G. Christmann, P. Lefebvre, J.-D. Ganière, N. Grandjean, and B. Deveaud-Plédran, Phys. Rev. B **85**, 245308 (2012).
[22]W. G. Scheibenzuber, U. T. Schwarz, R. G. Veprek, B. Witzigmann, and A. Hangleiter, Phys. Rev. B **80**, 115320 (2009).
[23]I. Vurgaftman and J. R. Meyer, J. Appl. Phys. **94**, 3675 (2003).
[24]R. P. Leavitt and J. W. Little, Phys. Rev. B **42**, 11774 (1990).
[25]S. A. Moskalenko, Fiz. Tverd. Tela **4**, 276 (1962) [Sov. Phys.–Solid State **4**, 199 (1962)].
[26]H. Hanamura and H. Haug, Phys. Rep. **33**, 209 (1977).
[27]A. V. Kavokin, J. J. Baumberg, G. Malpuech, and F. P. Laussy, *Microcavities* (Oxford University Press, Oxford, 2007).
[28]M. Kira, F. Jahnke, S. W. Koch, J. D. Berger, D. V. Wick, T. R. Nelson Jr., G. Khitrova, and H. M. Gibbs, Phys. Rev. Lett. **79**, 5170 (1997).
[29]N. F. Mott, Philos. Mag. **6**, 287 (1961).
[30]R. Houdré, J. L. Gibernon, P. Pellandini, R. P. Stanley, U. Oesterle, C. Weisbuch, J. O'Gorman, B. Roycroft, and M. Ilegems, Phys. Rev. B **52**, 7810 (1995).
[31]W. H. Knox, R. L. Fork, M. C. Downer, D. A. B. Miller, D. S. Chemla, C. V. Shank, A. C. Gossard, and W. Wiegmann, Phys. Rev. Lett. **54**, 1306 (1985).
[32]R. Zimmermann, Phys. Status Solidi B **146**, 371 (1988).
[33]H. Reinholz, Solid State Commun. **123**, 489 (2002).
[34]Y. E. Lozovik and O. L. Berman, Phys. Scripta **55**, 491 (1997).
[35]G. Manzke, D. Semkat, and H. Stolz, New J. Phys. **14**, 095002 (2012).
[36]H. Schweizer, A. Forchel, A. Hangleiter, S. Schmitt-Rink, J. P. Löwenau, and H. Haug, Phys. Rev. Lett. **51**, 698 (1983).
[37]H. W. Yoon, M. D. Sturge, and L. N. Pfeiffer, Solid State Commun. **104**, 287 (1997).
[38]A. Amo, M. D. Martin, L. Viña, A. I. Toropov, and K. S. Zhuravlev, Phys. Rev. B **73**, 035205 (2006).
[39]L. Kappei, J. Szczytko, F. Morier-Genoud, and B. Deveaud, Phys. Rev. Lett. **94**, 147403 (2005).
[40]P. Bigenwald, A. V. Kavokin, B. Gil, and P. Lefebvre, Phys. Rev. B **63**, 035315 (2001).
[41]M. Leroux, N. Grandjean, M. Laugt, J. Massies, B. Gil, P. Lefebvre, and P. Bigenwald, Phys. Rev. B **58**, R13371 (1998).
[42]S. Kalliakos, P. Lefebvre, and T. Taliercio, Phys. Rev. B **67**, 205307 (2003).
[43]N. Peyghambarian, H. M. Gibbs, J. L. Jewell, A. Antonetti, A. Migus, D. Hulin, and A. Mysyrowicz, Phys. Rev. Lett. **53**, 2433 (1984).
[44]F. Tassone and Y. Yamamoto, Phys. Rev. B **59**, 10830 (1999).
[45]S. Schmitt-Rink, C. Ell, S. W. Koch, H. E. Schmidt, and H. Haug, Solid State Commun. **52**, 123 (1984).
[46]D. A. Kleinman and R. C. Miller, Phys. Rev. B **32**, 2266 (1985).
[47]W. W. Chow, A. Girndt, and S. W. Koch, Opt. Express **2**, 119 (1998).
[48]U. T. Schwarz, E. Sturm, W. Wegscheider, V. Kümmler, A. Lell, and V. Härle, Appl. Phys. Lett. **85**, 1475 (2004).
[49]S. Wachter, M. Maute, H. Kalt, and I. Galbraith, Phys. Rev. B **65**, 205314 (2002).
[50]S. Utsunomiya, L. Tian, G. Roumpos, C. W. Lai, N. Kumada, T. Fujisawa, M. Kuwata-Gonokami, A. Löffler, S. Höfling, A. Forchel, and Y. Yamamoto, Nat. Phys. **4**, 700 (2008).
[51]J. K. Rhee, D. S. Citrin, T. B. Norris, Y. Arakawa, and M. Nishioka, Solid State Commun. **97**, 941 (1996).
[52]B. Deveaud, F. Clérot, N. Roy, K. Satzke, B. Sermage, and D. S. Katzer, Phys. Rev. Lett. **67**, 2355 (1991).
[53]K. Litvinenko, D. Birkedal, V. G. Lyssenko, and J. M. Hvam, Phys. Rev. B **59**, 10255 (1999).
[54]Biexcitonic emission has been traced particularly for low-Al content high-quality GaN/AlGaN QWs (Ref. 55), but often remains absent for higher-Al contents. There are two likely reasons for this: (i) the high-Al content causes an increased inhomogeneous linewidth, which potentially prohibits the formation and observation of QW biexcitons due to disorder, and (ii) the rising impact of the QCSE might hamper the biexciton formation (Ref. 56). This latter explanation could apply for the present case, where despite a comparable Al content and inhomogeneous linewidth biexcitons remain absent in the broader single QW, whereas it is well observed in the narrow MQWs, where the homogeneous distribution of QWs also damps the impact of the QCSE (geometrical effect) (Ref. 57).
[55]F. S. Cheregi, A. Vinattieri, E. Feltin, D. Simeonov, J.-F. Carlin, R. Butté, N. Grandjean, and M. Gurioli, Phys. Rev. B **77**, 125342 (2008).
[56]F. Stokker-Cheregi, A. Vinattieri, E. Feltin, D. Simeonov, J. Levrat, J.-F. Carlin, R. Butté, N. Grandjean, and M. Gurioli, Appl. Phys. Lett. **93**, 152105 (2008).
[57]N. Grandjean, B. Damilano, S. Dalmasso, M. Leroux, M. Laügt, and J. Massies, J. Appl. Phys. **86**, 3714 (1999).
[58]The change in the cavity mode position due to the Kerr effect is negligible. Even when considering the highest peak power density used in this work, the relative refractive index variation $\Delta n_{\mathrm{cav}}/n_{\mathrm{cav}}$ can not account for a cavity mode energy shift larger than 0.1–1 meV, according to values reported in Ref. 59.

[59]Y. L. Huang, C. K. Sun, J. C. Liang, S. Keller, M. P. Mack, U. K. Mishra, and S. P. DenBaars, Appl. Phys. Lett. **75**, 3524 (1999).
[60]S. Pau, G. Björk, J. Jacobson, H. Cao, and Y. Yamamoto, Phys. Rev. B **51**, 14437 (1995).
[61]V. Savona, L. C. Andreani, P. Schwendimann, and A. Quattropani, Solid State Commun. **93**, 733 (1995).
[62]M. Wouters and I. Carusotto, Phys. Rev. Lett. **99**, 140402 (2007).
[63]I. Iorsh, M. Glauser, G. Rossbach, J. Levrat, M. Cobet, R. Butté, N. Grandjean, M. A. Kaliteevski, R. A. Abram, and A. V. Kavokin, Phys. Rev. B **86**, 125308 (2012).
[64]J. Levrat, G. Rossbach, A. Dussaigne, G. Cosendey, M. Glauser, M. Cobet, R. Butté, N. Grandjean, H. Teisseyre, M. Bockowski, I. Grzegory, and T. Suski, Phys. Rev. B **86**, 165321 (2012).
[65]J. Levrat, R. Butté, G. Christmann, E. Feltin, J.-F. Carlin, and N. Grandjean, Phys. Status Solidi C **6**, 2820 (2009).
[66]G. Christmann, D. Simeonov, R. Butté, E. Feltin, J.-F. Carlin, and N. Grandjean, Appl. Phys. Lett. **89**, 261101 (2006).
[67]G. Christmann, R. Butté, E. Feltin, J.-F. Carlin, and N. Grandjean, Phys. Rev. B **73**, 153305 (2006).
[68]An additional diaphragm in front of the UV objective restricted the angular collection of the micro-PL to $\pm 3^{\circ}$, while giving a slightly increased spot size. The Q factor was calculated using Eq. (7) and the known position and linewidth of the QW exciton.
[69]The simulations have been performed following Eqs. (6) and (9) and assuming $\gamma_C = 4$ meV, and $\gamma_X = k_B T$, $g_0 = 30$ meV, where k_B denotes the Boltzmann constant. The variation of $P_{thr}(T,\delta)$ was adopted from the experimental data of Ref. 16 using a 2D polynomial fit [cf. Fig. 7(b)].
[70]The exclusive presence of the nonlinear blue-shift mechanism at low carrier densities does not match with the nature of the CB process, which is expected to occur when the homogeneous linewidth overcomes the inhomogeneous one at high carrier densities (Ref. 52) and from Sec. IV A a distinct detuning impact would be expected.
[71]M. Wouters, Phys. Rev. B **76**, 045319 (2007).
[72]A. Huynh, J. Tignon, Ph. Roussignol, C. Delalande, R. André, R. Romestain, and D. Le Si Dang, Phys. Rev. B **66**, 113301 (2002).
[73]D. Bajoni, P. Senellart, E. Wertz, I. Sagnes, A. Miard, A. Lemaître, and J. Bloch, Phys. Rev. Lett. **100**, 047401 (2008).
[74]S. Kéna-Cohen and S. R. Forrest, Nat. Photonics **4**, 371 (2010).
[75]M. Slootsky, Y. Zhang, and S. R. Forrest, Phys. Rev. B **86**, 045312 (2012).
[76]G. Roumpos, W. H. Nitsche, S. Höfling, A. Forchel, and Y. Yamamoto, Phys. Rev. Lett. **104**, 126403 (2010).